Received: 18 December 2018 | Revised: 15 March 2019 | Accepted: 16 March 2019

DOI: 10.1002/jmor.20984

RESEARCH ARTICLE

JOURNAL OF morphology WILEY

Killing them softly: Ontogeny of jaw mechanics and stiffness in mollusk-feeding freshwater stingrays

Kelsi M. Rutledge[1,2] | Adam P. Summers[1] | Matthew A. Kolmann[3,4,1]

[1]Department of Biology, Friday Harbor Laboratories, University of Washington, Friday Harbor, Washington

[2]Department of Ecology and Evolutionary Biology, University of California, Los Angeles, California

[3]Department of Biological Sciences, George Washington University, Washington, D.C.

[4]Department of Ichthyology, Royal Ontario Museum, Toronto, Ontario

Correspondence
Kelsi M. Rutledge, Department of Ecology and Evolutionary Biology, University of California Los Angeles, Los Angeles, CA 90095.
Email: kelsi.rutledge@gmail.com; kelsimarie7@g.ucla.edu

Present address
Kelsi M. Rutledge, Department of Ecology and Evolutionary Biology, University of California Los Angeles, Los Angeles, CA 90095.

Funding information
Division of Biological Infrastructure, Grant/Award Numbers: 1712015, 1759637; Division of Environmental Biology, Grant/Award Number: 1701665; Friday Harbor Labs Wainwright Fellowship; Human Frontier Science Program; UCLA Research Grant; Seaver Institute, Grant/Award Numbers: 1701665, 1759637; NSF-DBI, Grant/Award Number: 1712015

Abstract

Durophagous predators consume hard-shelled prey such as bivalves, gastropods, and large crustaceans, typically by crushing the mineralized exoskeleton. This is costly from the point of view of the bite forces involved, handling times, and the stresses inflicted on the predator's skeleton. It is not uncommon for durophagous taxa to display an ontogenetic shift from softer to harder prey items, implying that it is relatively difficult for smaller animals to consume shelled prey. Batoid fishes (rays, skates, sawfishes, and guitarfishes) have independently evolved durophagy multiple times, despite the challenges associated with crushing prey harder than their own cartilaginous skeleton. *Potamotrygon leopoldi* is a durophagous freshwater ray endemic to the Xingu River in Brazil, with a jaw morphology superficially similar to its distant durophagous marine relatives, eagle rays (e.g., *Aetomylaeus*, *Aetobatus*). We used second moment of area as a proxy for the ability to resist bending and analyzed the arrangement of the mineralized skeleton of the jaw of *P. leopoldi* over ontogeny using data from computed tomography (CT) scans. The jaws of *P. leopoldi* do not resist bending nearly as well as other durophagous elasmobranchs, and the jaws are stiffest nearest the joints rather than beneath the dentition. While second moment has similar material distribution over ontogeny, mineralization of the jaws under the teeth increases with age. Neonate rays have low jaw stiffness and poor mineralization, suggesting that *P. leopoldi* may not feed on hard-shelled prey early in life. These differences in the shape, stiffness and mineralization of the jaws of *P. leopoldi* compared to its durophagous relatives show there are several solutions to the problem of crushing shelled prey with a compliant skeleton.

KEYWORDS
batoid, computed tomography, durophagy, Potamotrygonidae, Xingu River

1 | INTRODUCTION

The batoid fishes (rays, skates, sawfishes, and guitarfishes) occupy a wide spectrum of ecological niches, and represent more than half the species of cartilaginous fishes. This diversity in habitat and prey use is matched by specialized feeding modes, including insectivores, vermivores, planktivores, and even intraguild predation on other batoids (Dean, Bizzarro, Clark, Underwood, & Johanson, 2017; Dean, Bizzarro, & Summers, 2007; Jacobsen & Bennett, 2013). Elasmobranchs feed on a diverse prey assortment despite a cranial skeleton with few parts, using kinetic jaws suspended by the hyomandibular apparatus which allow for extreme jaw protrusion (>100% of head length), asymmetrical jaw muscle action, and even reconfiguration of the dentition in some taxa (Dean, Huber, & Nance, 2006; Dean & Motta, 2004; Dean, Ramsay, & Schaefer, 2008; Dean, Wilga, & Summers, 2005; Gerry, Ramsay, Dean, & Wilga, 2008). Perplexingly, durophagous chondrichthyans feed on prey

that have exoskeletons tougher, stiffer, or harder than their own jaws, a remarkable example of adaptations associated with consuming robust biomaterials (Jayasankar et al., 2017; Seidel et al., 2016).

Durophagy has evolved several times independently in batoid fishes, including in some guitarfishes (e.g., *Rhina*), skates, and several different stingray lineages, including all members of the subfamilies Aetobatinae, Myliobatinae, and Rhinopterinae (Aschliman, 2014; Dean et al., 2007; Enault, Cappetta, & Adnet, 2013). While durophagy is perhaps too broadly defined and includes the consumption of many kinds of shelled invertebrate prey, most durophagous predators share common morphological adaptations or "hallmarks." These typically include: robust tooth plates, jaws reinforced via cortical thickening or trabecular struts, fused jaw symphyses, and large jaw adductor muscles (Aschliman, 2014; Kolmann, Huber, Dean, & Grubbs, 2014; Summers, 2000). However, there is unrecognized diversity in the cranial morphology and feeding mechanics of durophagous rays, such as differences in the shape and curvature of the jaws and associated dental battery (Claeson et al., 2010; Kolmann et al., 2014; Kolmann, Crofts, Dean, Summers, & Lovejoy, 2015b).

The morphological diversity among durophagous batoids suggests that specialized niches merit correspondingly specialized morphologies and that phenotypic convergence may be common across Batoidea (Dean et al., 2007). However, durophagous batoids exhibit developmental and population-level differences in feeding morphology, implying both temporal and spatial changes in prey use (Collins, Heupel, Hueter, & Motta, 2007; Kolmann et al., 2018; Schluessel, Bennett, & Collin, 2010). Perhaps morphological diversity among durophagous batoids reflects nuances in the taxonomic composition or material properties of hard prey in the diet, or constraints on development of such robust morphologies (Kolmann et al., 2015b; Kolmann, Huber, Motta, & Grubbs, 2015a). The number of times similar dietary ecologies have arisen across Batoidea is a chance to test for patterns of convergence (similarity of form) or equifinality (similarity in function) among morphologies correlated with feeding performance.

Neotropical river rays (Potamotrygoninae) invaded the interior of South America during the Miocene, and are the only extant lineage of obligate freshwater cartilaginous fishes (Lovejoy, Albert, & Crampton, 2006; Lovejoy, Bermingham, & Martin, 1998). In this diverse clade, there are several examples of durophagy with disparate morphologies and feeding modes, including several of the few chondrichthyan species known to consume insects: *Potamotrygon motoro* (Moro, Charvet, & Rosa, 2012a, 2012b; Kolmann, Welch, Summers, & Lovejoy, 2016). The Xingu River Ray (*Potamotrygon leopoldi*, Castex & Castello, 1970) is endemic to the Xingu River Basin in Brazil and it feeds largely on gastropods (Charvet-Almeida, Silva, Rosa, & Barthem, 2005). Perhaps unsurprisingly, jaws of *P. leopoldi* are more morphologically similar to those of the obligate hard prey specialists, the myliobatine stingrays (Figure 1), than the jaws of its close relative, *P. motoro* (Fontenelle, Loboda, Kolmann, & de Carvalho, 2017).

The difficulty of crushing hard prey with a compliant skeleton is at odds with the frequency with which cartilaginous fishes feed on this type of prey: nacreous, chitinous, or otherwise. Are all durophagous chondrichthyans cut from the same cloth? If specialized niches necessitate specialized morphologies, we expect strong selection for similar forms with similar functions. Alternatively, combinations of select traits of the many durophagous "hallmarks" could be sufficient for feeding on hard-shelled prey. We examined anatomical traits of the molluscivorous *P. leopoldi* relative to other durophagous chondrichthyans to access differences in jaw development. The purpose of this study is to (a) assess functional changes in the jaw lever

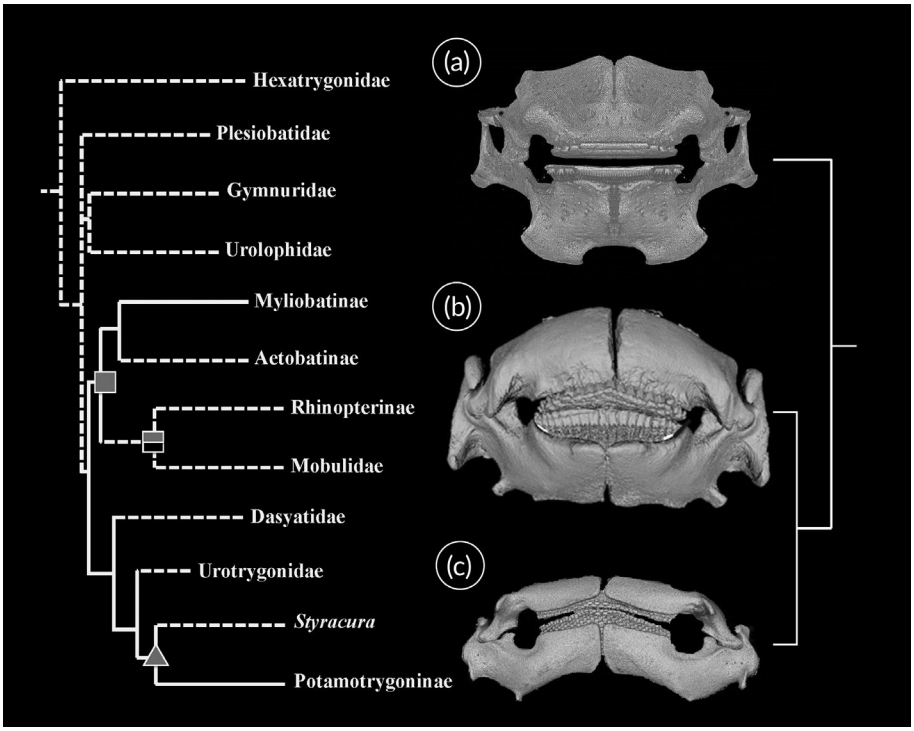

FIGURE 1 Comparison of jaws from durophagous stingrays (Myliobatiformes). (a) *Myliobatis freminvillei* jaws, (b) *Potamotrygon leopoldi* jaws, (c) *Potamotrygon motoro* jaws. Grey triangle denotes the marine and freshwater members of Potamotrygonidae. Grey square indicates the Myliobatidae, while the half-grey/half-black square represents the paraphyly of Myliobatidae without inclusion of the planktivorous Mobulidae. Dotted lines in the left phylogeny represent branches not shown on the right. Branch lengths not to scale. Phylogeny modified from Aschliman et al., 2012 and Aschliman, 2014

TABLE 1 Museum accession numbers for freshwater river ray specimens used in this study

Specimen accession number	Disc width (cm)
ANSP 198643	14
ANSP 197001	16
ROM 84398	19.5
ANSP 193061	44
ANSP 194503	45

mechanics, stiffness, mineralization, and dentition of *P. leopoldi* over ontogeny, (b) describe the myology of this species, (c) determine how many times molluscivory and other durophagous feeding modes have arisen across Batoidea, and (d) compare and evaluate whether shared morphological traits among these durophagous lineages suggest equivalency in either form (convergence) or function (equifinality).

2 | METHODS

2.1 | Specimen acquisition and micro-computed tomographic scanning

An ontogenetic series of Xingu River rays (*Potamotrygon leopoldi* Castex & Castello, 1970; *n* = 5; 14–45 cm DW) were obtained from collections at the Royal Ontario Museum (ROM) and the Academy of Natural Sciences of Drexel University (ANSP; Table 1). The specimens obtained for this study were collected through funding provided by the iXingu project (DEB-1257813). We measured disc width (DW) by hand, while head length was measured through CT-scans. Smaller specimens were wrapped in alcohol-saturated cheesecloth, placed in 3D-printed PLA (polylactic acid) plastic tubes for scanning, and then encased with plastic wrap to prevent desiccation. Larger specimens were also wrapped in ethanol-moistened cheesecloth and thick plastic wrapping and were sandwiched between two 5 cm thick panels of insulation foam, held tight by masking tape. Smaller specimens were scanned using a Skyscan 1,173 micro-source computed tomography scanner (μCT; Bruker, Billerica, MA) at the Karel F. Liem Bio-imaging Facility at Friday Harbor Laboratories, Friday Harbor, WA. Larger specimens were scanned at the University of Washington Mechanical Engineering Department on their Nikon Metrology scanner. Smaller scans used X-ray beam settings ranging from 65–70 kV and 110–123 uA, with a 1 mm aluminum (Al) filter, from 31 to 65 μm voxel size. Larger scans used X-ray settings of 120 kV and 160 uA, a 1 mm Al filter, and 65 μm magnification.

To compare the gross jaw muscle anatomy of *P. leopoldi* to other durophagous chondrichthyans we CT-scanned iodine contrast enhanced specimens to visualize soft tissues. X-ray imaging techniques image radiodense skeletal tissues such as bone and enamel. We modified the iodine contrast-staining method of Gignac and Kley (2014), to take advantage of the high molecular weight of iodine to visualize muscle tissue. The smallest ray (ANSP 198643, 14 cm DW) was stained with a 3% Lugol's solution (i.e., 0.75% I_2 and 1.5% of KI in 70% EtOH) for 24 hr to capture the gross structure and position of the jaw muscles. Scans were reconstructed to reduce ring-artifacts, beam-hardening, and postalignment shifts using and were visualized and segmented using the open-source platform, 3D-Slicer (www.slicer.org).

2.2 | Second moment of area calculations and jaw mineralization

We estimated the jaw's second moment of area (*I*), the measure of the distribution of the material around the neutral axis (or centroid) of a shape, as our biomechanical proxy for resistance to bending. It can be calculated as the sum of the distance squared of an area from the neutral axis. The neutral axis is a line perpendicular to the applied force that passes through the centroid of the cross section (Figure 2).

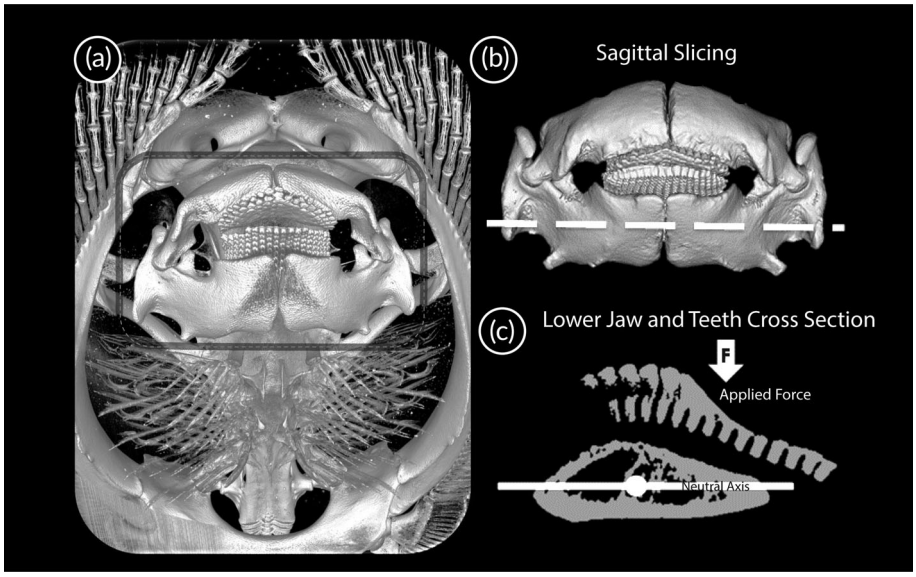

FIGURE 2 Computed tomography images of *Potamotrygon leopoldi* showing second moment of area orientation and neutral axis. (a) Cranial anatomy of *Potamotrygon leopoldi*, grey rectangle encloses upper and lower jaws (courtesy of M. Dean, J. Weaver, and M. Kolmann). (b) Isolated upper and lower jaws, large dashed line indicates the direction in which cross sectional slices where taken. (c) An example of one of the many sagittal cross sectional slices through the lower jaw; arrow with "F" denotes where crushing force is applied. Solid line indicates the minor or neutral axis used in second moment calculations, while the circle represents the centroid of the jaw shape

$$I = \int y^2 dA \quad (1)$$

We serially segmented jaws from CT-slice data, isolating the upper and lower jaws (palatoquadrate and Meckel's cartilage) using the "Editor" module in 3D-Slicer (Fedorov et al., 2012). To obtain a cross sectional view, we virtually resliced the right upper and lower jaws along their long axes using the "Reslice" tool in Fiji (Schindelin et al., 2012). Second moment of area calculations were performed on the upper and lower jaw of every CT-slice for all specimens using BoneJ (Doube et al., 2010). The threshold tool was used for a binary greyscale conversion of the entire image stack. This allows for the program to code the jaw as white pixels and the background as black pixels. BoneJ then automatically determines the centroid of the jaw shape and displays this as the point of intersection of two axes aligned with the best fit ellipse. The program counts each of the white pixels and their distance from the major and minor axes to compute two second moments. From the position of the teeth on the jaw, we can infer the direction of the crushing force applied during eating, since the neutral axis is perpendicular to this direction of force, and in this case, in line with the minor axis. These values are roughly comparable between scans because Summers, Ketcham, and Rowe (2004) show that within a visually reasonable range of thresholds, there is little difference in second moment.

Following Summers et al. (2004), we took the ratio of the second moment area of the jaw to the second moment area of a circle with the same area (Herbert & Motta, 2018; Macesic & Summers, 2012). This provides a unitless number that captures how well the jaw resists bending relative to a ciruclar rod with identical mineral investment. Second moment area of a circle is given by: $I = (\pi r^4)/4$.

Finally, we analyzed differences in skeletal mineralization along the jaw by comparing pixel brightness values between two distinctive jaw regions, the region supporting the dentition and the region adjacent to it (from the lateral teeth to the jaw joint) in 3D-Slicer. Brighter pixel values represent more mineralized regions while darker values represent less-mineralized tissues. We expected the skeleton supporting the dentition to be more mineralized than the adjacent jaw skeleton. We calculated a ratio from measures of pixel values in these two skeletal regions and examined how regional jaw mineralization changed over ontogeny.

2.3 | Jaw muscle morphology and jaw leverage

One hallmark of predatory durophagous chondrichthyans is hypertrophy of the jaw adductor musculature (Huber, Eason, Hueter, & Motta, 2005; Mara, Motta, & Huber, 2010). We compared the gross cranial myology of *P. leopoldi* to published morphological data in other potamotrygonids (Carvalho & Lovejoy, 2011; Lovejoy, 1996; Shibuya, Zuanon, & Tanaka, 2012). Myological and gross anatomical terminology follows Miyake, McEachran, and Hall (1992) and Kolmann et al. (2014). We identified insertions, origins, and fiber architecture of the jaw muscles using CT-data from our iodine-stained specimen (ANSP 198643). We both manually and virtually dissected specimens of *P. leopoldi*, the latter by segmenting the jaw and other cranial muscles using 3D-Slicer.

We measured linear morphometrics to assess functional changes in jaw lever mechanics and dentition of these stingrays over ontogeny, using the 3D-MPR function in 3D-Slicer. We calculated mechanical advantage, a proxy for the efficiency of force transmission (leverage) from insertion of the jaw adductors to where prey is crushed, a ratio of in-lever to out-lever distances. Batoid jaws are not shaped like those of sharks or even most other vertebrates, as they are wider than they are long. We use "medial" to denote regions of the jaws nearest the symphysis (e.g., medial symphysis) versus "lateral," which we use to describe jaw regions nearest to and culminating at the jaw joints. So, when using medial or lateral mechanical advantage, it refers to the leverage at more medial (symphyseal) or lateral regions of the jaw.

Jaw-closing in-lever distances were measured from the insertion of the primary jaw adductors (AM major and lateralis) on the lower jaw to the position of the jaw joint (as confirmed by Lugol's-stained and dissected specimens). Out-lever distances were measured from the jaw joint to where force is applied to prey, typically an anterior-most tooth. Stingrays have overt regions of the dentition where teeth are considerably worn through interactions with prey. The anterior-most and lateral-most extent of this tooth wear were used as the distal points of our closing out-lever measurements (sensu Kolmann et al., 2015a). Mechanical advantage can also describe the efficiency of jaw opening, that is, how the hypaxial muscles depress and retract the lower jaw. For opening mechanical advantage, the in-lever was measured from the insertion of the coracomandibularis on the medial symphysis of the Meckel's cartilage to the jaw joint.

2.4 | Evolutionary comparisons among durophagous batoids

We counted how many times different "durophagous" diets (e.g., molluscivory, crustacivory, insectivory) evolved across the batoid tree. We first trimmed one of the phylogenetic trees generated by Stein et al. (2018) to a genus-level tree (using their 10 fossil calibrations tree), constrained the topology at the ordinal level (according to the more robust backbone from Aschliman et al., 2012), and only used those taxa for which diet data were available (see Table S1). We then classified taxa according to whether they were durophagous or non-durophagous; if over 50% of a taxon's gut contents were comprised of a particular kind of shelled prey (e.g., mollusks, echinoderms, insects, decapod crustaceans), we considered this species to be durophagous. We then used stochastic character mapping and maximum likelihood methods to generate an ancestral state reconstruction of durophagous feeding traits across the phylogeny of Batoidea using the *ace* and *make.simmap* functions in the packages [ape] and [phytools] (Paradis, Claude, & Strimmer, 2004; Revell, 2012).

2.5 | Durophagous chondrichthyans in morphological space

We trimmed the Aschliman et al. (2012) tree to include only the following durophagous chondrichthyans for which morphological data are also available: *Hydrolagus colliei* (Huber, Dean, & Summers, 2008),

TABLE 2 Morphological matrix of scored, discrete characters for principal components analysis of durophagous chondrichthyans

Traits ↓ taxa →	*Hydrolagus colliei*	*Heterodontus francisci*	*Sphyrna tiburo*	*Rhina anclyostoma*	*Myliobatis freminvillei*	*Aetobatus narinari*	*Rhinoptera bonasus*	*Potamotrygon leopoldi*
Jaw 2nd moment of area	Low	High	High	Unknown	High	High	High	Intermediate
Fused jaw symphyses	Absent	Absent	Absent	Unknown	Present	Present	Present	Absent
Molariform dentition	Complete	Partial	Partial	Complete	Complete	Complete	Complete	Complete
Jaw muscle hypertrophy	Absent	Present	Absent	Unknown	Absent	Present	Present	Present
Trabeculae	Absent	Absent	Absent	Present	Present	Present	Present	Present
Jaw mechanical advantage	High	High	Low	Unknown	High	High	High	Intermediate

Some trait data were not available for *Rhina anclyostoma*, so to account for missing data an imputed principal components analysis was used to ordinate and group durophagous taxa within the morphospace.

Heterodontus francisci (Huber et al., 2005; Kolmann & Huber, 2009), *Sphyrna tiburo* (Herbert & Motta, 2018; Mara et al., 2010), *Rhina anclyostoma*, *Myliobatis freminvillei* and *Aetobatus narinari*, *Rhinoptera bonasus* (Kolmann et al., 2018), and *Potamotrygon* (*P. leopoldi*). We built a morphological matrix of scored, discrete characters including whether taxa had (a) jaws with high second moment of area, (b) fused jaw symphyses, (c) molariform dentition across the entire or partial jaw region, (d) hypertrophied muscles (relative to congeners), (e) jaws supported by internal trabeculation, and (f) high mechanical advantage either in the anterior or posterior jaw region (Summers, 2000; Summers et al., 2004; Huber et al., 2005; Huber et al., 2008; Mara et al., 2010; Herbert & Motta, 2018; Kolmann et al., 2018; Table 2). Complete sets of trait data were not available for some of the genera, so we used an imputed principal components analysis to ordinate and group durophagous taxa within a morphospace. This PCA uses an imputation method to account for missing or "gappy" data, executed through the *imputePCA* function in [FactoMineR] (Lê, Josse, & Husson, 2008). We then used the *phylomorphospace* function in [phytools] (Revell, 2012) to visualize where durophagous taxa fall within "trait space" and the variables factor map to examine associations between different sets of anatomical hallmarks.

3 | RESULTS

3.1 | Second moment of area

The second moment of area (I; mm^4) of the upper and lower jaws of *P. leopoldi* was highest at the lateral jaw joint throughout ontogeny, suggesting the jaw shape under the joint is best at resisting flexion (Figure 3). The medial symphysis of the two jaw elements was lowest in second moment throughout ontogeny. Moving sagittally through the lower jaw from right to left, there was an increase in second moment at the lateral region where the upper and lower jaws join, followed by a sharp decrease and then an increase right before the region of the jaw supporting a tooth plate and another decrease to the medial symphysis of the lower jaw (Figure 4a). The upper jaw

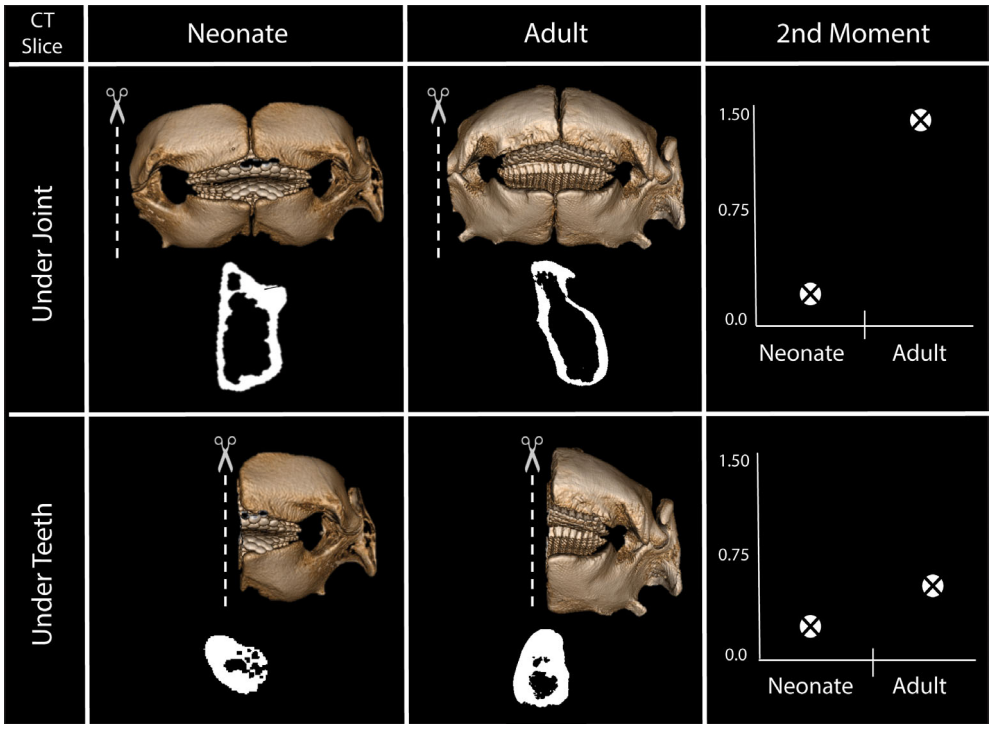

FIGURE 3 Differences in lower jaw material orientation and second moment of area (mm^4) in two regions for neonate and adult *Potamotrygon leopoldi*; showing sagittal CT-slices under the jaw joint (top panel) and directly under the teeth (bottom panel). Adults have a more optimal arrangement of skeletal material for resisting load perpendicular to the occlusal plane at both jaw regions. The region under the jaw joint had the higher second moment of area

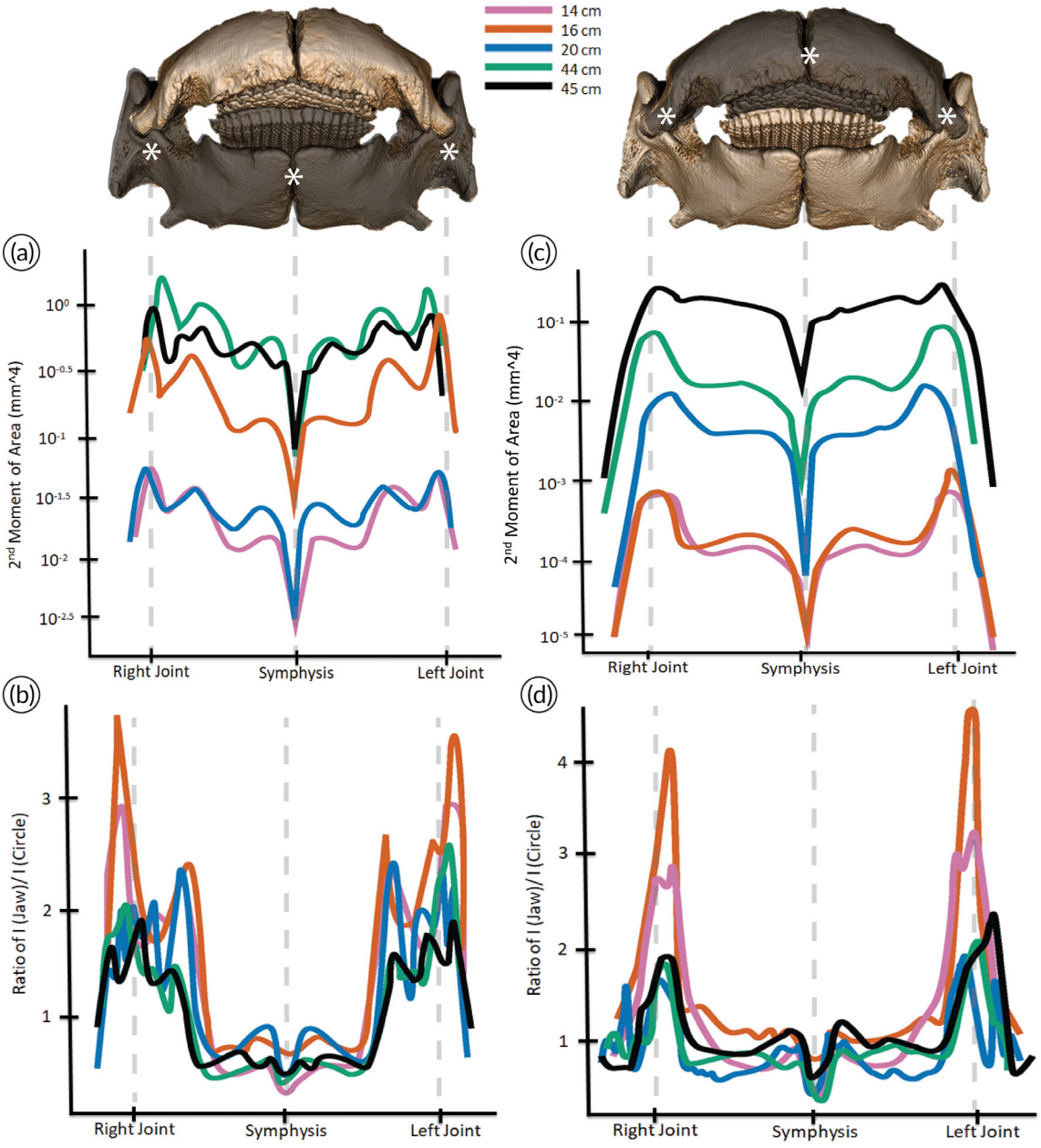

FIGURE 4 Second moment of area (mm^4) of the lower (a) and upper (c) jaws of *Potamotrygon leopoldi*. Ratios of second moment of area of the lower (b) and upper (d) jaws to that of a circular rod (I_{jaw}/I_{circle}) of *Potamotrygon leopoldi*. Colored lines represent the different sized rays measured by disc width through ontogeny; pink representing the neonate and black representing the fully grown adult, other colors are intermediate sizes. Arrangement of skeletal material is better at resisting bending near the jaw joints and declines in effectiveness medially toward the medial jaw symphyses

followed a similar pattern to the lower jaw, but with a consistently lower second moment of area, and the peak in second moment right before the tooth plate was absent (Figure 4c).

The neonate ray (14 cm) had the smallest second moment throughout the entire region of the lower jaw, with a peak in second moment at the region of the lateral joint of 0.07 mm^4 (Figures 3 and 4a). The slightly larger ray (16 cm) had a larger second moment throughout the lower jaw, with a peak in second moment at the region of the lateral joint of 0.35 mm^4 (Figure 4a). The largest rays (44–45 cm) had the highest second moment throughout the lower jaw, with a peak in second moment at the region of the joint of 1.2 mm^4 (Figures 3 and 4a). The upper jaws had slightly lower second moment of area, with the largest ray having a peak in second moment at the region of the joint of 0.30 mm^4 (Figures 4c).

The dimensionless ratio of the second moment of the jaws to that of a cylindrical rod (I_{jaw}/I_{circle}) was similar in pattern for all stages in ontogeny, ranging from 0.8 to 3.5 for the lower jaws (Figure 4b) and 0.5 to 4 for the upper (Figure 4d). The neonate rays (14–16 cm) had the largest second moment ratio at the region of the lower jaw joint of 3.5 but the lowest second moment ratio at the region of the lower jaw

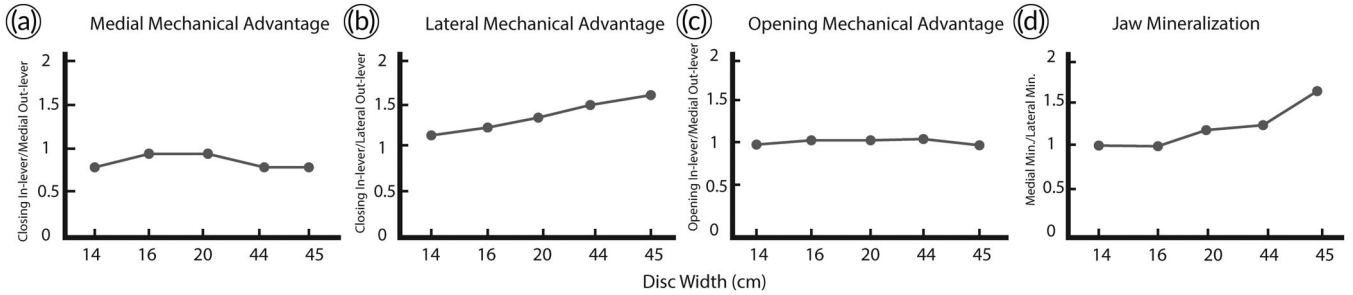

FIGURE 5 Mechanical advantage (a–c) and mineralization ratios (d) of *Potamotrygon leopoldi* through ontogeny. (a) Medial mechanical advantage: Jaw closing mechanical advantage at medial symphysis. (b) Lateral mechanical advantage: Jaw closing mechanical advantage at lateral extent of dentition. (c) Opening mechanical advantage. (d) Mineralization ratio: Ratio of the mineralization under the teeth when compared to the mineralization under the jaw joint

under the teeth of 0.8 (Figure 4b). The two largest rays (44–45 cm) had the smallest second moment ratio at the region of the lower jaw joint and the largest second moment under the region with the teeth (Figure 4b). The upper jaws followed a similar pattern but had generally higher second moment ratios under the joint when compared to the lower jaw (Figure 4d).

3.2 | Lever mechanics

The closing in-lever increased in length nearly fourfold (1.1–4.3 cm) over ontogeny (Figure 5a–c). The opening in-lever increased as well, from 1.6 cm in the neonate to 6.2 cm in the largest adult. The medial and lateral out-levers increased as well (med.: 1.6–6.1 cm; lat.: 0.9–2.8 cm). However, these increases were not gradual: the three smallest rays all had proportionally similar, yet shorter lever lengths, while the adult levers increased to be nearly threefour fold larger. Thus, closing medial mechanical advantage generally remained static over ontogeny, from neonate to adult. Lateral mechanical advantage increased through ontogeny, with an increase in lateral mechanical advantage ratio of 1.25 to 1.54 through development. The opening mechanical advantage remained consistent across ontogeny, ranging from a ratio of 1.0 to 1.2.

3.3 | Mineralization

The mineralization of the jaws increased through ontogeny. The ratio of the mineralization under the teeth when compared to the mineralization under the jaw joint increased with disc width (Figure 5d). The mineralization ratio increased gradually with development (1.0 at 14 cm DW to 1.56 at 45 cm DW). The increase in mineralization from neonate to adult was evident in the pixel brightness of CT-scan slices (Figure 6). Trabeculae were also found in the lateral margins of the jaws in medium-sized and adult specimens (20–45 DW), but were not obvious in CT-scans of neonates or small juveniles (14–16 DW; Figure 7).

3.4 | Myology

In dasyatoids, the adductor mandibulae major (AMMa) and adductor mandibulae lateralis (AMLa) adduct the upper and lower jaws together and appear to act together as a pennate muscle unit and are noticeably hypertrophied in *P. leopoldi* (Figure 8). As in other dasyatoids, in *Potamotrygon* the AMMa and AMLa cover the entire jaw joint region,

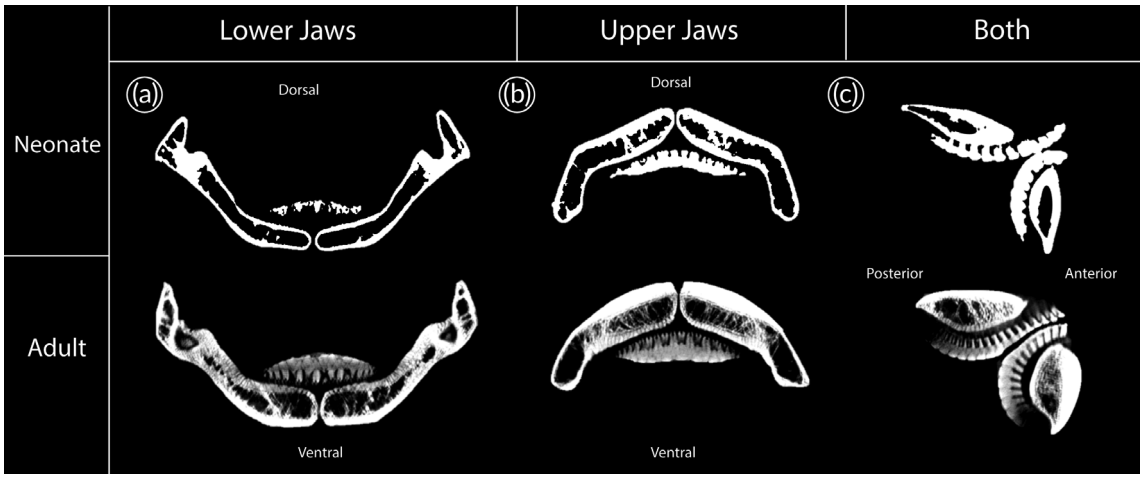

FIGURE 6 Increasing mineralization in the jaw skeleton of 14 cm disc width neonate (top panel) vs. 45 cm disc width adult (bottom panel) *Potamotrygon leopoldi*. (a) Lateral section of CT-slice of lower jaws. (b) Lateral section of CT-slice of upper jaws. (c) Sagittal section of CT-slice of upper and lower jaws

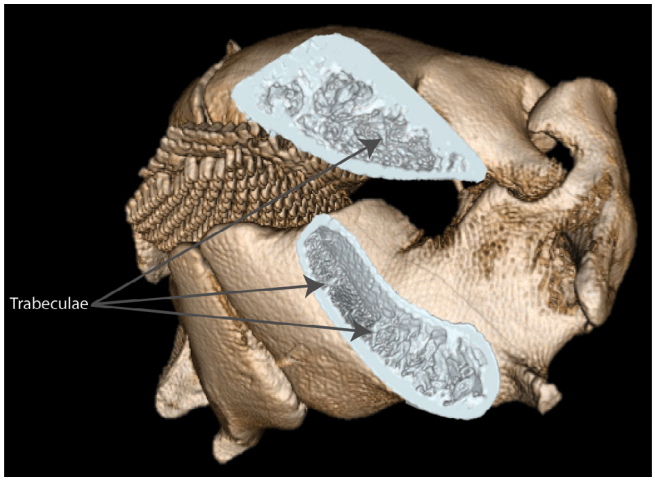

FIGURE 7 Trabeculae can be seen as bracing struts in the sagittal slices of the jaws of a 45 cm disc width adult *Potamotrygon leopoldi*

with both muscles originating far anterior on the palatoquadrate. The AMMa originates on the anterior lateral curvature of the palatoquadrate and inserts via a shared tendon on the ventral posterior region of the Meckel's cartilage. The AMLa originates on the anterolateral processes of the palatoquadrate (dorsal surface) and shares a common tendinous insertion with the suborbitalis on the Meckel's cartilage. The AMLa also broadly inserts along the lateral half of the ventral fossa of the Meckel's cartilage, while the AMMa occupies the medial half. Adductor mandibulae medialis (AMMe): In *Potamotrygon*, *Dasyatis*, and *Urobatis* the AMMe wraps around the corners of the mouth, originating on the palatoquadrate on either side of the dentition, and inserting in mirrored position on the Meckel's cartilage. This muscle constrains the lateral gape during jaw protrusion by associating with the labial cartilages.

We were not able to locate the lingualis (AMLi) or deep (AMD) divisions of the adductor mandibulae in *Potamotrygon*, corroborating previous observations regarding dasyatoid myology (Kolmann et al., 2014). The closing in-lever insertion was considered where the AMMa and AMLa insert on the posterior margin of the Meckel's cartilage. The opening in-lever inserts medial to the aforementioned in-lever insertion, where the two rami of the Meckel's cartilages meet (i.e., at the posterior-most region of medial lower jaw symphysis).

The hypaxial series muscles include the coracoarcualis (CARC), coracomandibularis (CM), coracohyoideus (CH), and coracohyomandibularis (CHYM), with the latter unique to batoids (Kolmann et al., 2014; Miyake et al., 1992). The CARC and CM abduct the lower jaw and

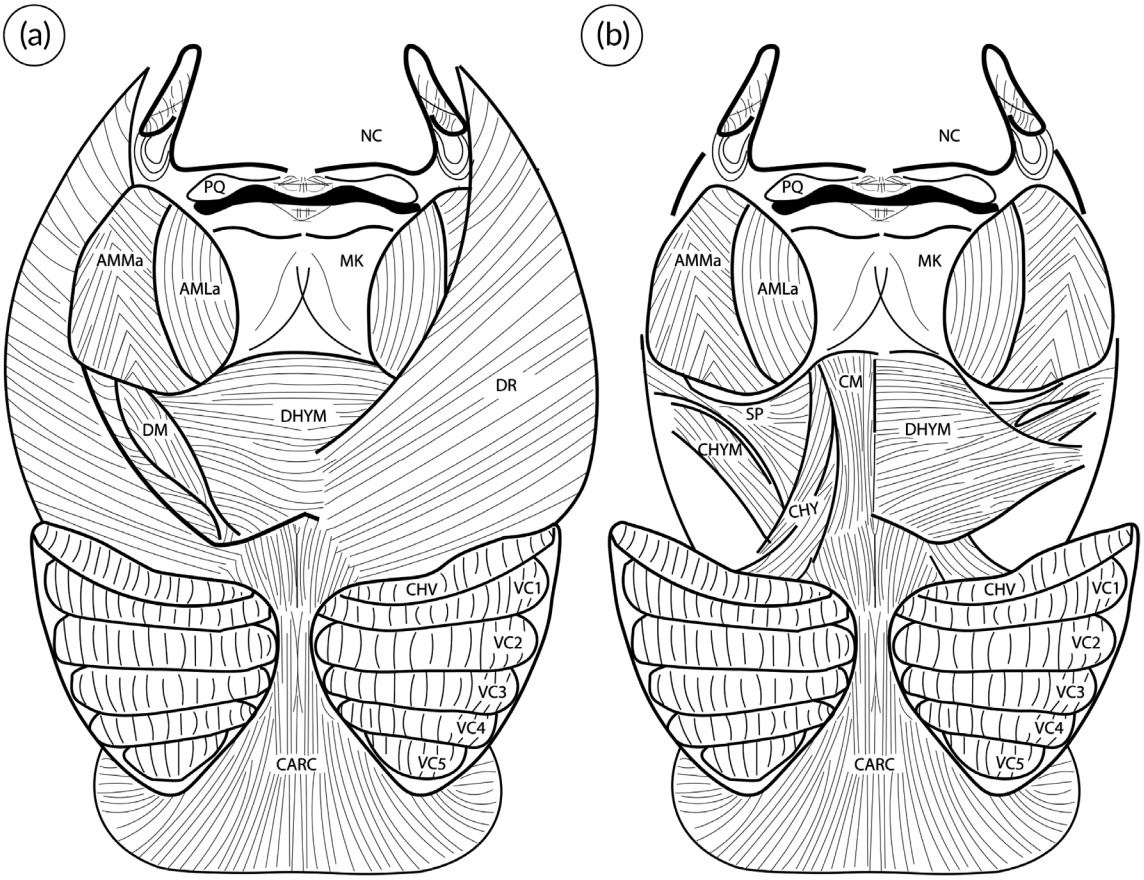

FIGURE 8 Superficial (a) and deep (b) cranial myology of ventral *Potamotrygon leopoldi*. Depressor rostri reflect on the left side of (a) Depressor hyomandibularis reflected on left side of (b) Abbreviations: AMLa, Adductor mandibulae lateralis, AMMa, Adductor mandibulae major, CARC, Coracoarcualis, CM, Coracomandibularis, CHY, Coracohyoideus, CHYM, Coracohyomandibularis, DHYM, Depressor hyomandibularis, DM, Depressor mandibularis, DR, Depressor rostri, MK, Meckel's cartilage, NC, Nasal curtain, PQ, Palatoquadrate, SB, Suborbitalis, SP, Spiracularis, VC1-5, Ventral gill arch constrictors

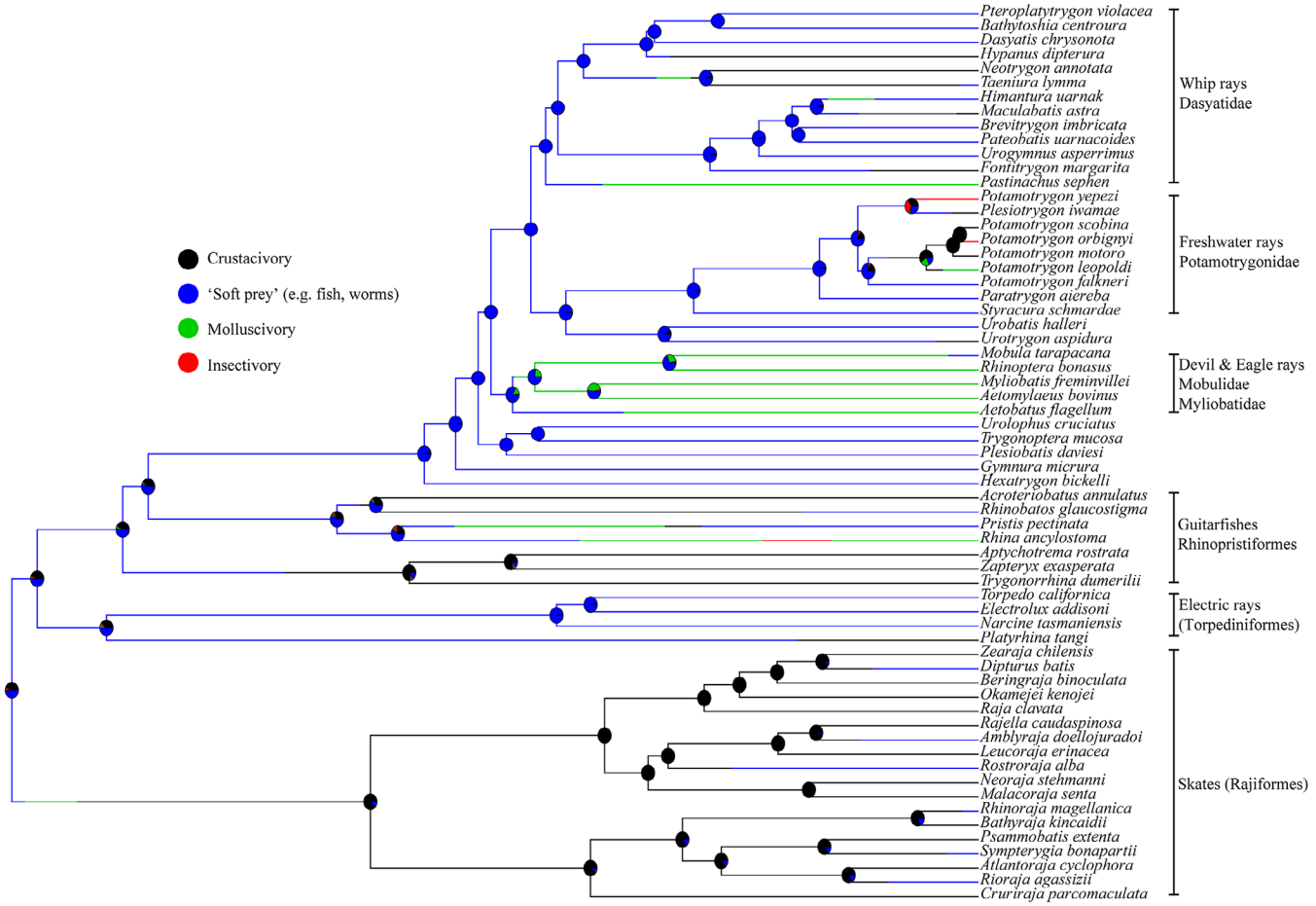

FIGURE 9 Ancestral state reconstruction of durophagous feeding modes across batoid genera. Blue represents soft prey specialization (fish, squid, worms, etc.), black indicates decapod crustacivory, red indicates insectivory, and green represents molluscivory. Skates and guitarfishes rely heavily on decapod crustaceans, while electric rays and stingrays evolved diets notably featuring piscivory, vermivory, and cephalopod-feeding (generalized as "soft" prey; O'Shea, Thums, Van Keulen, Kempster, & Meekan, 2013). Dietary specializations for mollusk-feeding appear to be largely restricted to myliobatiform stingrays. Tree modified from Stein et al. (2018)

are similar in position in all batoids. In *Potamotrygon*, the CARC and CM are paired muscles that are aligned in series. The CARC originates on the coracoid bar and insert on the CM. The CM originates on the anterior CARC and insert on the medial posterior margin of the Meckelian rami.

3.5 | Macroevolutionary patterns of durophagous chondrichthyans

Durophagous dietary modes, particularly decapod crustacivory, are widespread among the Batoidea (Figure 9). "Durophagous" crustacivory was coded in this study for those species feeding primarily on macrocrustaceans, for example, decapods like carideans and brachyurans. Crustacivory is particularly widespread among batoids, especially in skates (Rajiformes) and guitarfishes (Rhinopristiformes), more than in electric rays (Torpediniformes) and stingrays (Myliobatiformes). Molluscivory has evolved at least three times and as many as six, depending on whether durophagy in myliobatids stems from an evolutionary singularity (as has been traditionally assumed; see Summers, 2000; Aschliman, 2014) or represents multiple parallel instances of molluscivory (Kolmann et al., 2015b). Insectivory has evolved more than once within the freshwater Potamotrygoninae, but is not represented in any other batoid lineage (Kolmann et al., 2016).

The morphospace shows that selachian, holocephalan, and batoid durophages overwhelmingly group with regards to clade affinity, with little evident convergence among clades (Figure 10; Table 3). Jaws with high second moment of area loaded highly on PC1, while those taxa with fused jaw symphyses loaded positively on PC1, PC2. Taxa with jaws fully covered with molariform teeth loaded highly on PC2, while those with hypertrophied muscles also loaded positively on PC1. Finally, those taxa with jaws supported by internal trabeculae loaded highly on PC1, and those taxa with high jaw leverage (mechanical advantage) loaded highly on PC2. The PCA vector map suggests that some durophagous hallmarks are found associated with each other more often than others, for example, taxa with high mechanical advantage also tended to have molariform teeth (over the entirety of the jaw) and fused jaw symphyses. Alternatively, durophagous chondrichthyans with large muscles also tend to have trabeculae supporting the jaws, but perhaps not fused symphyses.

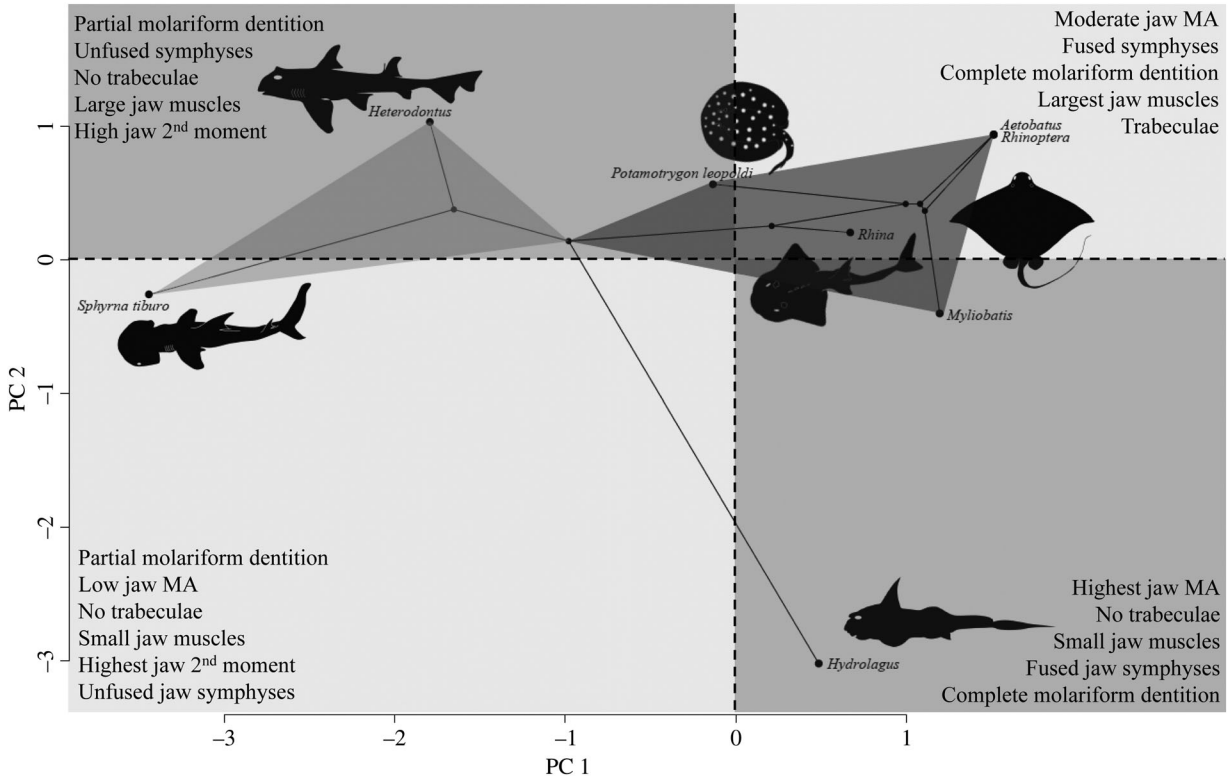

FIGURE 10 Character morphospace of durophagous chondrichthyans. Light grey convex hull encompasses durophagous elasmobranchs, *Sphyrna tiburo* and *Heterodontus francisci*, while the darker grey convex hull encompasses durophagous batoids, myliobatid stingrays *Aetobatus*, *Myliobatis*, *Rhinoptera*, rhinopristiform guitarfishes (*Rhina*), and the dasyatoid stingray *Potamotrygon leopoldi*. Character differences among durophagous chondrichthyans is largely split along phylogenetic axes, with the elasmobranch superorders, sharks and batoids, being more similar to one another than to holocephalans. Tree modified from Aschliman et al. (2012)

4 | DISCUSSION

The freshwater stingray *Potamotrygon leopoldi* possesses many characteristic traits of durophagous batoids including crushing molariform teeth, hypertrophied jaw closing muscles, reinforcing trabeculae, and a high mechanical advantage. However, the second moment of area, a proxy for resistance to bending of the jaws, was much lower than in other durophagous chondrichthyans (Herbert & Motta, 2018; Summers et al., 2004). This low resistance to bending, coupled with the unfused medial jaw symphyses, suggests there are multiple strategies used by durophagous chondrichthyans when it comes to crushing hard prey; *P. leopoldi* is not convergent with other durophagous elasmobranchs.

Furthermore, *P. leopoldi* is not well equipped to start life as a hard-prey specialist; compared to adults, neonate *P. leopoldi* had low jaw stiffness, little mineralization, and no obvious reinforcing trabeculae. Changes in the morphology and mineralization of the teeth from neonates to adults are apparent, with neonates possessing rounder and less-mineralized teeth (Figure 11). This shift in tooth morphology over ontogeny likely corresponds to a shift in prey type. While there are no studies on ontogenetic diet changes in *P. leopoldi*, these patterns in second moment, mineralization, and the underlying morphology of the jaws indicate these rays are mechanically constrained and unlikely to eat hard-shelled snails at small sizes. Changes in prey preference over development is not uncommon in durophagous chondrichthyans; previous studies suggest substantial changes in resource use, including horn

TABLE 3 Principle component analysis loadings based on the six morphometric and mechanical characters analyzed for durophagous chondrichthyans

Traits ↓ PC axes →	PC1 45.3%|2.72	PC2 26.1%|1.57	PC3 13.4%|0.8	PC4 13.2%|0.79	PC5 1.9%|0.18
Jaw second moment of area	−0.062	0.639	5.000	0.149	0.000
Fused jaw symphyses	0.501	−0.249	0.397	0.204	0.646
Molariform dentition	0.548	−0.163	−0.114	−0.381	−0.005
Jaw muscle size	0.163	0.614	−0.616	0.145	0.442
Trabeculae	0.458	0.355	0.114	−0.510	−0.341
Jaw mechanical advantage	0.456	−0.020	−0.104	0.714	−0.520

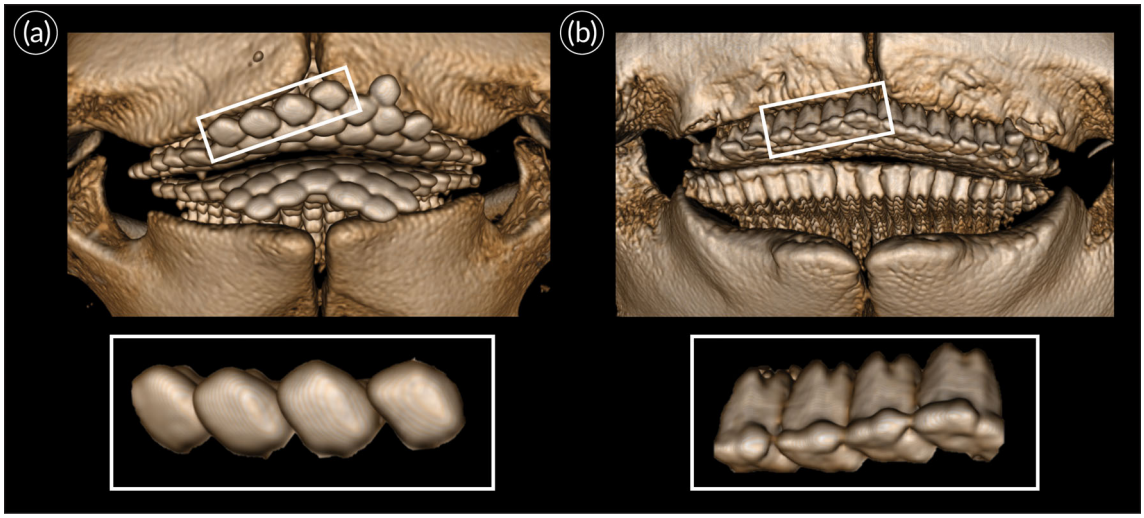

FIGURE 11 Ontogenetic changes in tooth shape in *Potamotrygon leopoldi*. (a) Teeth with rounded occlusal surfaces in 14 cm disc width specimen then (b) transition to a more tightly interlocking pavement-like dentition in a 45 cm disc width specimen; reminiscent of other durophagous myliobatiforms

sharks, bonnetheads, and myliobatid rays (Edmonds et al., 2001; Kolmann & Huber, 2009; Mara et al., 2010; Ajemian & Powers, 2012).

While a general increase in the stiffness, mineralization, and reinforcement of the jaws of a durophagous organism with size is not surprising, the patterns of stiffness seen in the jaws of *P. leopoldi* are. In other rays, the region of the jaw supporting the dentition, that is, where crushing takes place, is the most resistant to bending (Summers, 2000; Summers et al., 2004). *P. leopoldi* displays the opposite pattern, and while its jaws appear robust and morphologically similar to that of eagle rays and cownose rays, the second moment of area analysis revealed that the jaws of *P. leopoldi* are built more like durophagous sharks. The jaws of both horn sharks and bonnetheads display the same pattern as *P. leopoldi*, with an increasing second moment of area near the jaw joint (Herbert & Motta, 2018; Summers et al., 2004). Horn sharks and *P. leopoldi* also have similar lateral and posterior mechanical advantages (MA); *P. leopoldi* has ~1.5 lateral MA while the horn shark has a posterior MA of ~1.3 (Kolmann & Huber, 2009). This increase in second moment and mechanical advantage found in shark jaws correlates with heterodonty; specifically, a change from grasping to crushing teeth. It is likely that these sharks crush their food in the posterior region of their jaws, where the teeth and stiffness is best suited to do so (Summers et al., 2004).

Potamotrygon leopoldi is an outlier in the sense that its jaws are not stiffest where prey-crushing occurs; however, the relatively higher second moment values near the jaw joints may act to dissipate stresses built up under the teeth by transmitting forces along the jaw or by providing a broad region for muscle and/or tendon insertion (Summers, 2000; Summers et al., 2004). Elasmobranch cartilages have gradient mechanical properties between the most mineralized and least mineralized parts of the skeleton: depending on scale, having either a skeleton without true sutures (compared to bony vertebrates) or with thousands of tiny sutures (in between mineralized tesserae), which allow for optimization of multiple material properties (Jayasankar et al., 2017). Without "true" sutures (from a bony skeleton perspective) to expand and dissipate stresses, this continuum of material properties along mineralized cartilage may allow different regions of the same skeletal structure to act as stress dissipaters (i.e., the region adjacent to teeth; Tseng & Wang, 2010; Porter, Ewoldt, & Long, 2016; Seidel et al., 2016; Jayasankar et al., 2017). Perhaps distributing stresses widely along broad regions of the skeleton is a biomechanical motif for elasmobranchs. A related example is the higher frequency of aponeurotic muscle insertions and the comparable rarity of direct tendinous insertions in elasmobranchs: sharks and rays seem constrained to use broad regions of the skeleton for muscle attachment, stemming in part from the low pull-out strength of cartilage (but see Summers, 2000; Kolmann, Huber, et al., 2015a).

Differences in prey material properties, as well as the morphologies of the predators that consume them, underline the nebulous nature of "hard" prey and durophagy in general. *P. leopoldi* is nested within a family known for consuming mostly infaunal, softer-bodied invertebrates, epibenthic fishes, and the occasional decapod crustacean (Moro et al., 2012a, 2012b; Shibuya, Araújo, & Zuanon, 2009; Figure 8). Dasyatoid rays in general (e.g., Potamotrygonidae, Urotrygonidae, Dasyatidae, Urolophidae) are almost exclusively soft-bodied prey specialists (Jacobsen & Bennett, 2013), so *P. leopoldi* may be adapting jaws constrained by phylogenetic inertia for a new task: dismantling tough, hard, nacreous shell material. This is in stark contrast to the strategies employed by other "hard" prey consuming potamotrygonines like insectivorous *P. motoro* and *P. orbignyi*, which use highly-kinetic jaws to shear apart tough insect chitin (Kolmann et al., 2016). Not only are the materials that comprise insect and mollusk skeletons not analogous, their predators lie on either end of a morphological continuum.

What do durophagous chondrichthyans have in common? Each durophagous taxon's configuration of "hallmarks" has more to do with what these taxa inherit from their ancestors, as well as the specific material nature of their prey, rather than morphological or perhaps even

functional convergence. If equifinality is where two phenotypes result in a similar function, and convergence is where two lineages have a similar phenotype, with river rays, we see partial evidence for convergence in form or function (compared to the nearest mollusk-eating batoids or other durophagous chondrichthyans). For example, in the Xingu ray the jaw symphyses are not fused (*contra* eagle rays) and the arrangement of skeletal material in the jaws is very different from other durophagous rays (e.g., *Aetobatus*, *Myliobatis*); however, the mechanical advantage of the jaws is comparable with other durophagous batoids and the jaw muscles of *P. leopoldi* are noticeably larger than those of their non-durophagous congeners (as in other durophagous batoids). So, the phenotypic and functional outcome for durophagy in the Xingu river ray are an imperfect example of convergence (Collar, Reece, Alfaro, Wainwright, & Mehta, 2014) and equifinality. The jaws of *P. leopoldi* demonstrate one of the several ways to build a hard-prey specialist from parts already in the archetypal phylogenetic "toolbox."

ACKNOWLEDGMENTS

The authors thank Meredith Rivin (UW) for her assistance and time CT-scanning large specimens, Mark Sabaj and Mariangeles Arce-H. (ANSP) for preparing and shipping large specimens to us, as well as Erling Holm, Don Stacey and Marg Zur (ROM) who sent us specimens. A Human Frontiers in Science Funding (HFSP) to Mason Dean and James Weaver allowed for one of the images in Figure 2. We thank Cassandra Donatelli and Sarah Hoffman for assistance with scanning, software usage, and project logistics. KMR is supported by a FHL Wainwright Fellowship and UCLA Research Grant. MAK was supported by an NSF-DBI 1712015 Post-Doctoral Research Fellowship in Biology. APS was supported by the Seaver Institute, NSF DBI-1759637 and DEB-1701665. We would also like to thank two anonymous reviewers and the editor, Matthias Starck, for their necessary improvements to this manuscript.

CONFLICT OF INTEREST

The authors declare no conflicts of interest.

ORCID

Kelsi M. Rutledge https://orcid.org/0000-0002-2396-4764
Adam P. Summers https://orcid.org/0000-0003-1930-9748
Matthew A. Kolmann https://orcid.org/0000-0001-9748-2066

REFERENCES

Ajemian, M. J., & Powers, S. P. (2012). Habitat-specific feeding by cownose rays (*Rhinoptera bonasus*) of the northern Gulf of Mexico. *Environmental Biology of Fishes*, *95*(1), 79–97.

Aschliman, N. C. (2014). Interrelationships of the durophagous stingrays (Batoidea: Myliobatidae). *Environmental Biology of Fishes*, *97*(9), 967–979.

Aschliman, N. C., Nishida, M., Miya, M., Inoue, J. G., Rosana, K. M., & Naylor, G. J. (2012). Body plan convergence in the evolution of skates and rays (Chondrichthyes: Batoidea). *Molecular Phylogenetics and Evolution*, *63*(1), 28–42.

Castex, M. N., & Castello, H. P. (1970). *Potamotrygon leopoldi*: una nueva especie de raya de agua dulce para el Río Xingú, Brasil (Chondrichthyes, Potamotrygonidae). Departamento de Zoología, ILAFIR, Universidad del Salvador.

Charvet-Almeida, P., Silva, A. J. A., Rosa, R. S., & Barthem, R. B. (2005). Observações preliminares sobre a alimentação de *Potamotrygon leopoldi* (Potamotrygonidae) no médio rio Xingu - Pará. In Proceedings of 3 Workshop de Chondrichthyes do Núcleo de Pesquisa e Estudo em Chondrichthyes—NUPEC, Santos.

Claeson, K. M., O'Leary, M. A., Roberts, E. M., Sissoko, F., Bouaré, M., Tapanila, L., … Gottfried, D. (2010). First Mesozoic record of the stingray Myliobatis wurnoensis from Mali and a phylogenetic analysis of Myliobatidae incorporating dental characters. *Acta Palaeontologica Polonica*, *55*(4), 655–674.

Collar, D. C., Reece, J. S., Alfaro, M. E., Wainwright, P. C., & Mehta, R. S. (2014). Imperfect morphological convergence: Variable changes in cranial structures underlie transitions to durophagy in moray eels. *The American Naturalist*, *183*(6), E168–E184.

Collins, A. B., Heupel, M. R., Hueter, R. E., & Motta, P. J. (2007). Hard prey specialists or opportunistic generalists? An examination of the diet of the cownose ray, *Rhinoptera bonasus*. *Marine and Freshwater Research*, *58*, 135–144.

De Carvalho, M. R., & Lovejoy, N. R. (2011). Morphology and phylogenetic relationships of a remarkable new genus and two new species of Neotropical freshwater stingrays from the Amazon basin (Chondrichthyes: Potamotrygonidae). *Zootaxa*, *2776*, 13–48.

Dean, M. N., Bizzarro, J. J., Clark, B., Underwood, C. J., & Johanson, Z. (2017). Large batoid fishes frequently consume stingrays despite skeletal damage. *Royal Society Open Science*, *4*(9).

Dean, M. N., Bizzarro, J. J., & Summers, A. P. (2007). The evolution of cranial design, diet, and feeding mechanisms in batoid fishes. *Integrative and Comparative Biology*, *47*(1), 70–81.

Dean, M. N., Huber, D. R., & Nance, H. A. (2006). Functional morphology of jaw trabeculation in the lesser electric ray *Narcine brasiliensis*, with comments on the evolution of structural support in the Batoidea. *Journal of Morphology*, *267*(10), 1137–1146.

Dean, M. N., & Motta, P. J. (2004). Anatomy and functional morphology of the feeding apparatus of the lesser electric ray, *Narcine brasiliensis* (Elasmobranchii: Batoidea). *Journal of Morphology*, *262*(1), 462–483.

Dean, M. N., Ramsay, J. B., & Schaefer, J. T. (2008). Tooth reorientation affects tooth function during prey processing and tooth ontogeny in the lesser electric ray, *Narcine brasiliensis*. *Zoology*, *111*(2), 123–134.

Dean, M. N., Wilga, C. D., & Summers, A. P. (2005). Eating without hands or tongue: Specialization, elaboration and the evolution of prey processing mechanisms in cartilaginous fishes. *Biology Letters*, *1*(3), 357–361.

Doube, M., Kłosowski, M. M., Arganda-Carreras, I., Cordeliéres, F., Dougherty, R. P., Jackson, J., … Shefelbine, S. J. (2010). BoneJ: Free and extensible bone image analysis in ImageJ. *Bone*, *47*, 1076–1079.

Edmonds, M. A., Motta, P. J., & Hueter, R. E. (2001). Food capture kinematics of the suction feeding horn shark, Heterodontus francisci. *Environmental Biology of Fishes*, *62*(4), 415–427.

Enault, S., Cappetta, H., & Adnet, S. (2013). Simplification of the enameloid microstructure of large stingrays (Chondrichthyes: Myliobatiformes): A functional approach. *Zoological Journal of the Linnean Society*, *169*(1), 144–155.

Fedorov, A., Beichel, R., Kalpathy-Cramer, J., Finet, J., Fillion-Robin, J.-C., Pujol, S., … Kikinis, R. (2012). 3D-slicer as an image computing platform for the quantitative imaging network. *Magnetic Resonance Imaging*, *30*(9), 1323–1341.

Fontenelle, J. P., Loboda, T. S., Kolmann, M., & de Carvalho, M. R. (2017). Angular cartilage structure and variation in Neotropical freshwater stingrays (Chondrichthyes: Myliobatiformes: Potamotrygonidae), with comments on their function and evolution. *Zoological Journal of the Linnean Society*, *20*, 1–22.

Gerry, S. P., Ramsay, J. B., Dean, M. N., & Wilga, C. D. (2008). Evolution of asynchronous motor activity in paired muscles: Effects of ecology, morphology, and phylogeny. *American Zoologist*, *48*(2), 272–282.

Gignac, P. M., & Kley, N. J. (2014). Iodine-enhanced micro-CT imaging: Methodological refinements for the study of the soft-tissue anatomy of post-embryonic vertebrates. *Journal of Experimental Zoology Part B: Molecular and Developmental Evolution*, *322*(3), 166–176.

Herbert, A. M., & Motta, P. J. (2018). Biomechanics of the jaw of the durophagous bonnethead shark. *Zoology*, *129*, 54–58.

Huber, D. R., Dean, M. N., & Summers, A. P. (2008). Hard prey, soft jaws and the ontogeny of feeding mechanics in the spotted ratfish *Hydrolagus colliei*. *Journal of the Royal Society, Interface*, *5*(25), 941–952.

Huber, D. R., Eason, T. G., Hueter, R. E., & Motta, P. J. (2005). Analysis of the bite force and mechanical design of the feeding mechanism of the durophagous horn shark *Heterodontus francisci*. *Journal of Experimental Biology*, *208*(18), 3553–3571.

Jacobsen, I. P., & Bennett, M. B. (2013). A comparative analysis of feeding and trophic level ecology in stingrays (Rajiformes; Myliobatoidei) and electric rays (Rajiformes: Torpedinoidei). *PLoS One*, *8*(8), e71348.

Jayasankar, A. K., Seidel, R., Naumann, J., Guiducci, L., Hosny, A., Fratzl, P., … Dean, M. N. (2017). Mechanical behavior of idealized, stingray-skeleton-inspired tiled composites as a function of geometry and material properties. *Journal of the Mechanical Behavior of Biomedical Materials*, *73*, 86–101.

Kolmann, M. A., Huber, D. R., Motta, P. J., & Grubbs, R. D. (2015a). Feeding biomechanics of the cownose ray, *Rhinoptera bonasus*, over ontogeny. *Journal of Anatomy*, *227*(3), 341–351.

Kolmann, M. A., Crofts, S. B., Dean, M. N., Summers, A. P., & Lovejoy, N. R. (2015b). Morphology does not predict performance: Jaw curvature and prey crushing in durophagous stingrays. *Journal of Experimental Biology*, *218*(24), 3941–3949.

Kolmann, M. A., Dean Grubbs, R., Huber, D. R., Fisher, R., Lovejoy, N. R., & Erickson, G. M. (2018). Intraspecific variation in feeding mechanics and bite force in durophagous stingrays. *Journal of Zoology*, *304*(4), 225–234.

Kolmann, M. A., & Huber, D. R. (2009). Scaling of feeding biomechanics in the horn shark *Heterodontus francisci*: Ontogenetic constraints on durophagy. *Zoology*, *112*(5), 351–361.

Kolmann, M. A., Huber, D. R., Dean, M. D., & Grubbs, R. D. (2014). Myological variability in a decoupled skeletal system: Batoid cranial anatomy. *Journal of Morphology*, *275*, 862–881.

Kolmann, M. A., Welch, K. C., Summers, A. P., & Lovejoy, N. R. (2016). Always chew your food: Freshwater stingrays use mastication to process tough insect prey. *Proceedings of the Royal Society B: Biological Sciences*, *283*, 20161392.

Lê, S., Josse, J., & Husson, F. (2008). FactoMineR: An R package for multivariate analysis. *Journal of Statistical Software*, *25*(1), 1–18.

Lovejoy, N. R. (1996). Systematics of myliobatoid elasmobranchs: With emphasis on the phylogeny and historical biogeography of neotropical freshwater stingrays (Potamotrygonidae: Rajiformes). *Zoological Journal of the Linnean Society*, *117*(3), 207–257.

Lovejoy, N. R., Albert, J. S., & Crampton, W. G. (2006). Miocene marine incursions and marine/freshwater transitions: Evidence from Neotropical fishes. *Journal of South American Earth Sciences*, *21*(1–2), 5–13.

Lovejoy, N. R., Bermingham, E., & Martin, A. P. (1998). Marine incursion into South America. *Nature*, *396*(6710), 421–422.

Macesic, L. J., & Summers, A. P. (2012). Flexural stiffness and composition of the batoid propterygium as predictors of punting ability. *Journal of Experimental Biology*, *215*(12), 2003–2012.

Mara, K. R., Motta, P. J., & Huber, D. R. (2010). Bite force and performance in the durophagous bonnethead shark, *Sphyrna tiburo*. *Journal of Experimental Zoology Part A: Ecological Genetics and Physiology*, *313*(2), 95–105.

Miyake, T., McEachran, J. D., & Hall, B. K. (1992). Edgeworth's legacy of cranial muscle development with an analysis of muscles in the ventral gill arch region of batoid fishes (Chondrichthyes: Batoidea). *Journal of Morphology*, *212*(3), 213–256.

Moro, G., Charvet, P., & Rosa, R. (2012b). Aspectos da alimentação da raia de água doce Potamotrygon orbignyi (Chondrichthyes: Potamotrygonidae) da bacia do rio Parnaíba, Nordeste do Brasil. *Revista Nordestina de Biologia*, *20*(2), 47–57.

Moro, G., Charvet, P., & Rosa, R. S. (2012a). Insectivory in *Potamotrygon signata* (Chondrichthyes: Potamotrygonidae), an endemic freshwater stingray from the Parnaíba River basin, northeastern Brazil. *Brazilian Journal of Biology*, *72*(4), 885–891.

O'Shea, O. R., Thums, M., Van Keulen, M., Kempster, R. M., & Meekan, M. G. (2013). Dietary partitioning by five sympatric species of stingray (Dasyatidae) on coral reefs. *Journal of Fish Biology*, *82*(6), 1805–1820.

Paradis, E., Claude, J., & Strimmer, K. (2004). APE: Analyses of phylogenetics and evolution in R language. *Bioinformatics*, *20*(2), 289–290.

Porter, M. E., Ewoldt, R. H., & Long, J. H. (2016). Automatic control: The vertebral column of dogfish sharks behaves as a continuously variable transmission with smoothly shifting functions. *Journal of Experimental Biology*, *219*(18), 2908–2919.

Revell, L. J. (2012). Phytools: An R package for phylogenetic comparative biology (and other things). *Methods in Ecology and Evolution*, *3*(2), 217–223.

Schindelin, J., Arganda-Carreras, I., Frise, E., Kaynig, V., Longair, M., Pietzsch, T., … Cardona, A. (2012). Fiji: An open-source platform for biological-image analysis. *Nature Methods*, *9*(7), 676–682.

Schluessel, V., Bennett, M. B., & Collin, S. P. (2010). Diet and reproduction in the white-spotted eagle ray *Aetobatus narinari* from Queensland, Australia and the Penghu Islands, Taiwan. *Marine and Freshwater Research*, *61*, 1278–1289.

Seidel, R., Lyons, K., Blumer, M., Zaslansky, P., Fratzl, P., Weaver, J. C., & Dean, M. N. (2016). Ultrastructural and developmental features of the tessellated endoskeleton of elasmobranchs (sharks and rays). *Journal of Anatomy*, *229*(5), 681–702.

Shibuya, A., Araújo, M. D., & Zuanon, J. A. (2009). Analysis of stomach contents of freshwater stingrays (Elasmobranchii, Potamotrygonidae) from the middle Negro River, Amazonas, Brazil. *Pan-American Journal of Aquatic Sciences*, *4*(4), 466–475.

Shibuya, A., Zuanon, J., & Tanaka, S. (2012). Feeding behavior of the Neotropical freshwater stingray *Potamotrygon motoro* (Elasmobranchii: Potamotrygonidae). *Neotropical Ichthyology*, *10*(1), 189–196.

Stein, R. W., Mull, C. G., Kuhn, T. S., Aschliman, N. C., Davidson, L. N., Joy, J. B., … Mooers, A. O. (2018). Global priorities for conserving the evolutionary history of sharks, rays and chimaeras. *Nature Ecology and Evolution*, *2*(2), 288–298.

Summers, A. P. (2000). Stiffening the stingray skeleton – An investigation of durophagy in myliobatid stingrays (Chondrichthyes, Batoidea, Myliobatidae). *Journal of Morphology*, *243*, 113–126.

Summers, A. P., Ketcham, R. A., & Rowe, T. (2004). Structure and function of the horn shark (*Heterodontus francisci*) cranium through ontogeny: Development of a hard prey specialist. *Journal of Morphology*, *260*(1), 1–12.

Tseng, Z. J., & Wang, X. (2010). Cranial functional morphology of fossil dogs and adaptation for durophagy in *Borophagus* and *Epicyon* (Carnivora, Mammalia). *Journal of Morphology*, *271*(11), 1386–1398.

SUPPORTING INFORMATION

Additional supporting information may be found online in the Supporting Information section at the end of this article.

How to cite this article: Rutledge KM, Summers AP, Kolmann MA. Killing them softly: Ontogeny of jaw mechanics and stiffness in mollusk-feeding freshwater stingrays. *Journal of Morphology*. 2019;280:796–808. https://doi.org/10.1002/jmor.20984